Hindawi
Advances in Materials Science and Engineering
Volume 2019, Article ID 3758527, 9 pages
https://doi.org/10.1155/2019/3758527

Research Article

Experimental Study on the Effects of Initial Shear Stress and Vibration Frequency on Dynamic Strength of Saturated Sands

Jian Zhang[1], **Jiuting Cao**[2] **and Sijie Huang**[3]

[1]*School of Architectural Engineering, Nanjing Institute of Technology, Nanjing 211167, China*
[2]*Jiangsu Zhongshe Group Co.,Ltd., Wuxi 214072, China*
[3]*Tianjin Institute of Water Transport Engineering, Ministry of Transport, Tianjin 300456, China*

Correspondence should be addressed to Jian Zhang; 18626439990@163.com

Received 13 August 2018; Revised 19 February 2019; Accepted 25 February 2019; Published 19 March 2019

Academic Editor: Ling B. Kong

The cyclic triaxial system is used to investigate the effects of confining pressure, initial shear stress, cyclic stress ratio, and vibration frequency on the dynamic strength characteristics of saturated sand in the Wenchuan area. Results show that when the vibration frequency is constant, the dynamic strength of sand increases with the increase of the consolidation ratio. However, when the consolidation ratio exceeds a certain value, the dynamic strength of sand decreases or increases slowly. The dynamic internal friction angle first increases and then decreases with the increase of consolidation ratio, and the dynamic internal friction angle under different initial shear stresses differs by a maximum of about 12%. When the failure cycles are constant, the dynamic strength and the dynamic internal friction angle of the sand increase with the increase of vibration frequency, and the dynamic internal friction angle at different frequencies differs by a maximum of about 7%. When the cyclic stress ratio is constant, the higher the vibration frequency, the greater the cycles required to achieve the failure. As the cyclic stress ratio decreases, the influence of the vibration frequency on the failure cycles is gradually reduced.

1. Introduction

China is an earthquake-prone country with a wide distribution of earthquakes. The earthquake in its southwestern part is particularly strong. In the past 100 years, the number of strong earthquakes ($M \geq 8$, in which M is earthquake amplitude) in China has reached 10 times, and casualties and property losses were severe in the densely populated area. In 1920, the number of deaths in the Haiyuan earthquake in Ningxia was more than 200,000, and the wounded were innumerable. In 1976, a 7.8-magnitude earthquake struck Tangshan, Hebei Province, where most of the urban houses collapsed, more than 240,000 people suffered, and the wounded were countless. In 2008, Wenchuan, Sichuan Province, suffered an 8.0-magnitude earthquake with a maximum intensity of 11 degrees. It covered a total of 10 provinces and cities, and its destructiveness and difficulty of relief were quite rare where more than 80,000 people were dead or missing, causing major casualties and property losses [1, 2].

A large number of earthquakes indicate that the liquefaction of saturated sand under the influence of earthquakes has caused great damage to pile foundations, embankments, slopes, and dams. Before the arrival of seismic loads, these structure foundations are often subjected to the initial shear stress due to the presence of upper structures [3, 4]. At present, most of the tests mainly consider the state where the initial shear stress does not exist, that is to start the test based on the equal three-dimensional consolidation pressure. The initial shear stress is an important factor, affecting the dynamic properties of saturated sands, and many researchers are beginning to pay attention to study the effect of initial shear stress [5–8].

Seed and Lee [9] pointed out that the internal friction angle of sand and the state transition angle marked by the initial dilatancy were stable soil properties, which were not affected by the cycles and the consolidation ratio. Yang and Sze [10] conducted an experimental study to investigate the undrained behavior of sand in nonsymmetrical cyclic

loading. The tests demonstrated that the presence of initial static shear stress was beneficial to the liquefaction resistance of loose sand at low initial shear stress ratio, but it became detrimental at high initial shear stress ratio. Georgiannou and Konstadinou [11] investigated the response of Ottawa sand to cyclic torsional loading under different densities and proposed that the cyclic strength resistance increased with the consolidation ratio and density, the rate of increase being higher for anisotropic consolidated specimens compared with isotropic consolidated specimens. Ma [12] explored the dynamic characteristics of Fujian standard sand at different consolidation ratios through dynamic triaxial tests. The study found that there was a certain value of K_c in which the dynamic strength of the sand increases with the increase of the consolidation ratio at first and the growth rate decreases gradually when the consolidation ratio exceeded a specific value. When the consolidation ratio reached 3.0, the dynamic strength began to decrease. Pan and Yang [13] investigated the combined effect of cyclic and static shears on the undrained cyclic response of sand. The results showed that the static shear effect on the cyclic resistance is influenced significantly by the relative density and mean normal stress of sand. Wang et al. [14] used dynamic triaxial tests to investigate the dynamic strength characteristics of sand pebble soil at different consolidation ratios. The study showed that the dynamic stress of sand pebble soil increased slightly with the increase of consolidation ratio, and dynamic strength increased significantly with the increase of confining pressure. Gao et al. [15] conducted a series of cyclic axial-torsional coupling tests simulating wave loads of different frequencies using a hollow cylinder instrument. The experimental results showed that as the consolidation ratio increased, the number of vibrations needed to reach the liquefaction of the saturated silt decreased, and the pore water pressure presented a "fast-steady-to-rapid" growth model. Cao et al. [16] conducted an undrained dynamic triaxial test on Wenchuan fine sand under different confining pressures and cyclic stress ratios and studied the relationship between the dynamic internal friction angle and the initial void ratio. The test results showed that when the void ratio was constant, the dynamic internal friction angle decreased and the liquefaction resistance was weaker as the failure cycles increased; under the same failure cycles, the smaller the void ratio, the larger the dynamic internal friction angle, and the stronger the liquefaction resistance of the sand. Huang and Cao [17] carried out cyclic triaxial tests on medium-density saturated sand under different consolidation ratios. The test results showed that when the cycle was constant, the greater the initial shear stress, the higher the dynamic strength of sand.

It can be seen from the above analysis that the earthquake caused a large number of sand foundations to be destroyed, and the initial shear stress is inevitable on these foundations. However, the influence of initial shear stress on the dynamic strength characteristics of saturated sand under seismic loading has not been consistently concluded. Therefore, it is necessary to further study the influence of initial shear stress. The obtained dynamic parameters can be used in structural dynamic analysis to provide a test basis for the stability analysis of sand foundation under seismic loading.

2. Soil Samples and Plans

2.1. Soil Samples. The sand used in the experiment was taken from Wenchuan, Sichuan, and the sampling depth was about 5 m. During the transportation process, the soil sample was disturbed and the natural state of the sand was not well controlled, so all the sand used in the test was remolded sand. The specific gravity of the test sand was $G_s = 2.66$, the maximum dry density ρ_{dmax} was 1.67 g/cm^3, and minimum dry density ρ_{dmin} was 1.22 g/cm^3, respectively. According to the natural density and water content of the sampling site, the relative compactness of the soil was kept as $D_r = 55\%$ and the dry density was kept as $\rho_d = 1.43$ g/cm^3. The sand gradation constants are shown in Table 1. The sand particle sieving curve is shown in Figure 1.

2.2. Test Procedures and Methods. The DDS-70 dynamic triaxial instrument used in this test was developed by Beijing New Technology Application Research Institute. The system equipment can carry out the dynamic characteristic test and dynamic elastic mode test to study the dynamic strength and dynamic deformation characteristics of soil.

The test used a remolded soil sample with a diameter of 39.1 mm and a height of 80 mm. The remolded soil sample was prepared using a multilayer wet mortar method and was divided into 5 layers for compaction. The weight of each layer was determined based on the dry density of the soil sample and the predesigned moisture content. Each layer was compacted to the corresponding height, and the contact surfaces were shaved to ensure good contact between layers. After the sample preparation, it was installed in the pressure chamber of the cyclic triaxial apparatus. In the pressure chamber, two methods were used to saturate the sample, i.e., vacuum pumping, airless water, and reversing pressure, which avoided the disturbance of the sample when the sample was placed in the vacuum saturation cylinder. When the pore water pressure coefficient B was ≥ 0.97, the sample was considered to meet the saturation requirement. In the consolidation phase, the drain valve was opened slowly after the saturation of the sample was completed. When the pore water pressure dissipated close to 0, the drain valve should be closed for 5 minutes. If the pore water pressure no longer rose, the consolidation was considered to be completed. After the isotropic consolidation was completed, the deviatoric stress was gradually increased. At this time, the drain valve should be opened to avoid deformation and damage. When applied to the corresponding deviatoric stress, it was consolidated for a period of time and then the drain valve was closed to complete the anisotropic consolidation process. The failure criteria used in this paper are the pore pressure criterion and the deformation criterion. Under the condition of isotropic consolidation, the failure criterion is that the pore water pressure is equal to the confining pressure; when the initial shear stress exists, the pore water pressure can not reach the confining pressure,

Table 1: Sand gradation constants.

Soil category	d_{60} (mm)	d_{50} (mm)	d_{30} (mm)	d_{10} (mm)	C_u	C_c
Sand	0.28	0.26	0.12	0.08	3.5	0.64

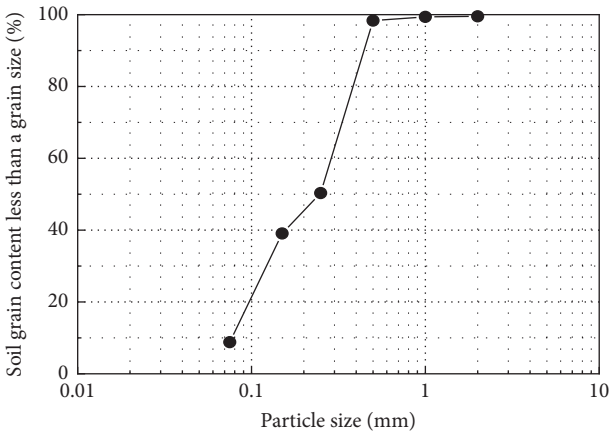

Figure 1: Sand particle sieving curve.

and the deformation criterion with a single strain of 5% is taken as the failure criterion [18].

2.3. Test Plans. According to the depth of soil extraction and research needs, consolidation confining pressures in this test are $\sigma_c = 50$ kPa, $\sigma_c = 100$ kPa, and $\sigma_c = 150$ kPa. Due to the short acting time of the cyclic loading provided by the earthquake, the drainage of the clay layer is slow, which can be considered that the soil is undrained, so the test used undrained shear. According to the frequency range of seismic loading, the vibration frequencies adopted are $f = 1$ Hz, $f = 2$ Hz, and $f = 3$ Hz. Due to the asymmetry and irregularity of seismic loading which is a typical random dynamic load, it is impossible to repeat the earthquake with the same seismic waveform. Therefore, the seismic loading input in this paper is simulated by the sine wave of equal amplitude waveform. The specific test plan is shown in Table 2. In order to consider the influence of initial shear stress on the dynamic characteristics of saturated sands, the dynamic triaxial tests of consolidation ratio $K_c = 1$, $K_c = 1.25$, and $K_c = 1.5$ are, respectively, carried out [18], in which

$$K_c = \frac{\sigma_{1c}}{\sigma_{3c}}, \tag{1}$$

where σ_{1c} and σ_{3c} are the major principal stress and minor principal stress, respectively, when the sample is consolidated [19–21].

3. Test Results and Analysis

The dynamic stress required to generate a specified failure criterion or meet a certain failure criterion when the soil is circulated under dynamic load is called the dynamic strength of the soil. The dynamic strength curve of soil is used to describe the relationship between dynamic stress and failure cycles, which reflects the corresponding relationship between the failure cycles and the dynamic stress of the soil under dynamic load. When the soil property is constant, the dynamic strength of the soil is determined by the static and dynamic conditions, the initial shear stress and the dynamic stress, and the vibration frequency. Therefore, the dynamic strength and dynamic strength indexes of saturated sand at different initial shear stresses and vibration frequencies are studied and analyzed [4, 5, 22, 23].

3.1. Effects of Initial Shear Stress on Dynamic Strength Characteristics of Saturated Sand. Figure 2 shows the dynamic strength curves of saturated sand affected by initial shear stress under different confining pressures. It can be seen from the test results that when the failure cycles is constant, the larger the initial shear stress, the larger the dynamic strength of the sand. It can be explained that when the initial shear stress is zero, the particle skeleton of the soil is in equilibrium, and the vibration will cause the shear stress to change direction repeatedly under the cyclic load, so that the soil particle skeleton is easy to slide, and the pore pressure rises faster and the dynamic strength is lower at this time. When the initial shear stress exists, the shear stress only changes in value, and there is no change or small change in direction, so that the deformation of the soil particle skeleton tends to be stable. At this time, the deformation rate and amplitude are reduced, and the pore pressure develops slowly and the dynamic strength increases.

Figure 3 shows the relationship between the cyclic stress ratio and the consolidation ratio at 10, 20, and 30 weeks of loading. It can be seen from Figure 3 that when the consolidation ratio increases from 1.0 to 1.5, the soil skeleton tends to be more stable, the cyclic stress ratio increases with the increase of consolidation ratio, the dynamic strength of sand is on the rise, and the increased value is 50%~60%; when the consolidation ratio exceeds 1.5, the soil quickly deforms and breaks after the dynamic load is applied, its dynamic strength decreases or increases slowly, and the increased value is only 5% to 10%. This indicates that as the initial shear stress increases to a certain extent, the dynamic strength of the soil sample will increase slowly with the increase of the consolidation ratio instead of increasing indefinitely.

When the initial shear stress exists, the major principal stress σ_{1d} and the minor principal stress σ_{3d} under dynamic failure conditions are, respectively, given by formula (2), and Mohr's circle is shown in Figure 4. The calculated dynamic strength indexes are shown in Table 3:

$$\left.\begin{aligned} \sigma_{1d} &= \sigma_{1c} + \sigma_d = \sigma_{3c} + \sigma_s + \sigma_d, \\ \sigma_{3d} &= \sigma_{3c}. \end{aligned}\right\} \tag{2}$$

Figure 5 shows the value of the dynamic strength parameters under different initial shear stresses when the frequency is 1 Hz. From the results, it can be seen that when the consolidation ratio ranges from 1 to 1.5, the dynamic internal friction angle increases with the increase of consolidation ratio, and the increased value can reach 15%; when the consolidation ratio ranges from 1.5 to 2, the

Table 2: Saturated sand dynamic strength test program.

Frequency f (Hz)	Lateral consolidation pressure σ_{3c} (kPa)	Initial shear stress σ_s (kPa)	Vertical consolidation pressure σ_{1c} (kPa)	Consolidation ratio K_c	Dynamic load σ_d (kPa)
1, 2, 3	50	0	50	1	41, 33, 25
1, 2, 3	100	0	100	1	83, 66, 50
1, 2, 3	150	0	150	1	125, 100, 75
1	50	25	75	1.5	58, 50, 41
1	50	50	100	2	66, 58, 50, 41
1	100	50	150	1.5	108, 100, 91
1	100	100	200	2	133, 116, 100, 91
1	150	75	225	1.5	200, 150, 120
1	150	150	300	2	210, 180, 150

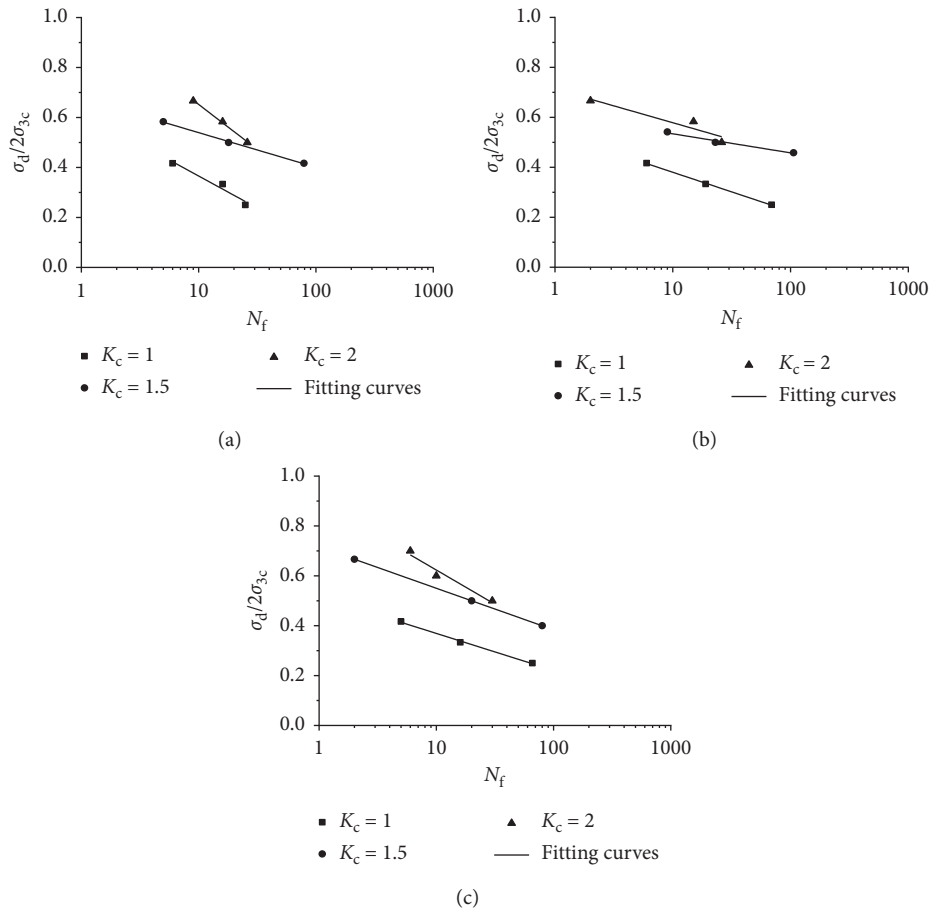

Figure 2: Relationship curves between cyclic stress ratio and failure cycles under different initial shear stresses at $f = 1$ Hz: (a) $\sigma_{3c} = 50$ kPa; (b) $\sigma_{3c} = 100$ kPa; (c) $\sigma_{3c} = 150$ kPa.

dynamic internal friction angle decreases with the increase of the initial shear stress, and the decreased value can reach 10%; the dynamic internal friction angle increases first and then decreases with the increase of the consolidation ratio; and the dynamic internal friction angle under different initial shear stresses differs by a maximum of about 12%. The dynamic friction angle of sand is the main source of dynamic strength. The variation of the dynamic friction angle with the consolidation ratio is consistent with the variation of the dynamic shear stress with the consolidation ratio, which can explain the variation law of dynamic strength.

3.2. Effects of Vibration Frequency on Dynamic Strength Characteristics of Saturated Sand. Figure 6 shows the relationship curves between the dynamic strength σ_d and failure cycles N_f when the sample is destroyed under different confining pressures. Under the same failure cycles, the larger the confining pressure, the larger the dynamic strength of the saturated sand, and the $\sigma_d \sim N_f$ relationship curve is linear on a single logarithmic axis; and under the same confining pressure, the failure cycles increase gradually with the decrease of dynamic stress, the curve reduction rate changes from fast to slow, and finally, the curve tends to be stable.

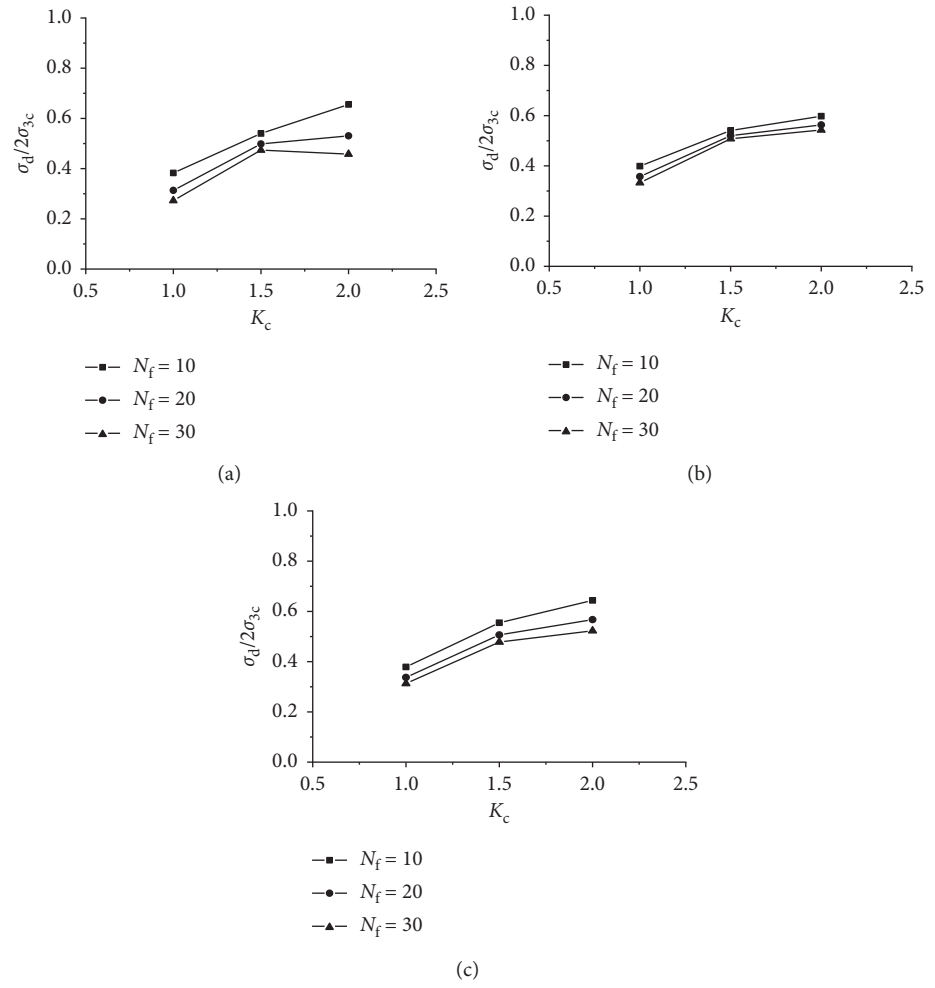

Figure 3: Relationship curves between cyclic stress ratio and consolidation ratio: (a) $\sigma_{3c} = 50$ kPa; (b) $\sigma_{3c} = 100$ kPa; (c) $\sigma_{3c} = 150$ kPa.

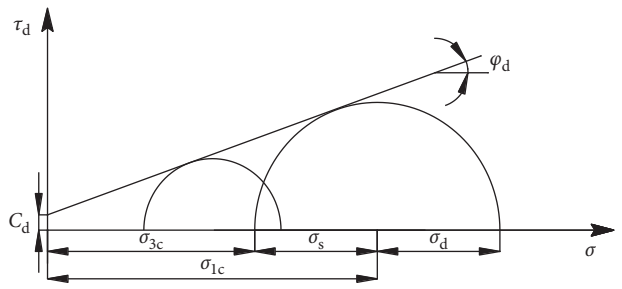

Figure 4: Schematic diagram of Mohr's circle and strength envelope under initial shear stress conditions.

Table 3: Dynamic strength indexes of saturated sand under different initial shear stresses.

K_c	1		1.5		2	
Cycles	φ_d (°)	c (kPa)	φ_d (°)	c (kPa)	φ_d (°)	c (kPa)
10	15.61	0	17.93	0	16.72	1.60
20	14.63	2.12	16.65	2.30	15.28	0
30	14.03	1.80	15.89	0	14.73	1.83

The relationship curves between the cyclic stress ratio and failure cycle at the different vibration frequencies are shown in Figure 7. It can be concluded that, under the same failure cycles, the greater the vibration frequency, the greater the dynamic strength of saturated sand, and the dynamic strength at $f = 3$ Hz is about 30%~40% higher than that at $f = 1$ Hz; at the same cyclic stress ratio, the higher the vibration frequency, the larger the cycles required to achieve the failure, and the failure cycles at $f = 3$ Hz is about 50%~60% higher than that at $f = 1$ Hz; and as the cyclic stress ratio decreases, the influence of the vibration frequency on failure cycles gradually decreases.

According to the dynamic strength curves, the dynamic stress σ_d required for failure cycles $N_f = 10$, 20, and 30 when the confining pressure and the vibration frequency are different can be obtained, and then the major principal stress σ_{1d} and minor principal stress σ_{3d} under the dynamic failure condition can be calculated according to formula (2).

As shown in Figure 8, Mohr's circle under failure cycles $N_f = 10$, 20, and 30 at vibration frequency $f = 1$ Hz, 2 Hz, and 3 Hz are given. The dynamic strength parameters corresponding to a certain vibration frequency and a certain failure cycles are obtained from Mohr's circle. The longitudinal intercept and slope of the Mohr's circle envelope

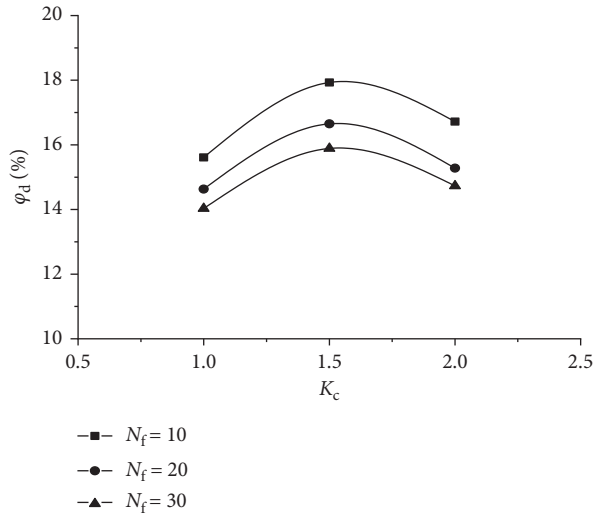

Figure 5: Curves of dynamic internal friction angle with consolidation ratio.

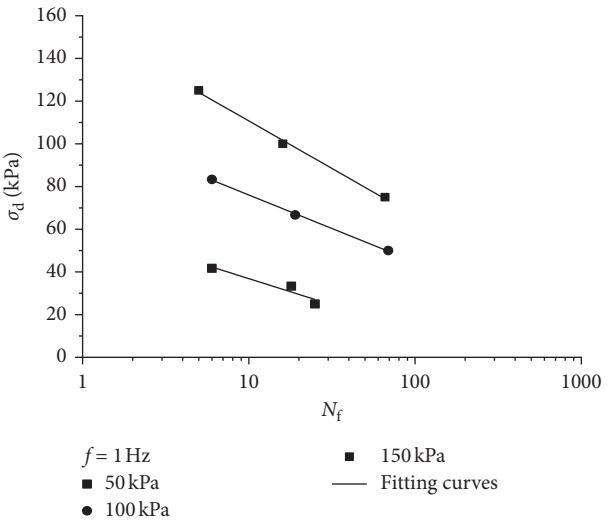

Figure 6: Relationship curves between dynamic strength and failure cycles at different frequencies.

indicate the dynamic cohesion c_d and the dynamic friction coefficient $\tan \varphi_d$, respectively.

Table 4 shows the dynamic internal friction angle φ_d and dynamic cohesion of saturated sand under failure cycles $N_f = 10$, 20, and 30 at each vibration frequency. It can be seen that the internal friction angle at different frequencies differs by a maximum of about 7% under the same failure cycles; at the same frequency, the internal friction angle at different failure cycles differs by a maximum of about 12%. This indicates that the internal friction angle is affected by failure cycles and vibration frequency. Wang et al. [13] considered that the internal friction angle was a stable soil index and was not affected by cycles, vibration frequency, and confining pressure.

The relationship between shear strength τ_f and normal stress σ under certain cycles can be expressed as follows:

$$\tau_f = c_d + \left(\frac{\sigma_1 - \sigma_3}{2}\right)\tan \varphi_d, \quad (3)$$

where c_d is the dynamic cohesion and φ_d is the dynamic internal friction angle. It can be seen from Table 4 that when the dynamic cohesion is close to zero, the shear strength of the soil under the influence of power can be approximately replaced by the following formula:

$$\tau_f = \left(\frac{\sigma_1 - \sigma_3}{2}\right)\tan \varphi_d. \quad (4)$$

The variation curve of the dynamic internal friction angle with the failure cycles of saturated sand is shown in Figure 9. The variation curve of the dynamic internal friction angle with the frequency of saturated sand is shown in Figure 10.

It can be seen from Figure 9 that when the vibration frequency is constant, as the cycles increases, the dynamic internal friction angle decreases. When the failure criterion is reached, the smaller the failure cycles, the greater the required dynamic stress, the stronger the friction between the soil particles, and the larger the internal friction angle of the sand. The higher the failure cycles, the smaller the required dynamic stress, and the friction between the particles decreases, so that the internal friction angle decreases.

It can be seen from Figure 10 that when the failure cycles is constant, the dynamic internal friction angle of the sand increases as the vibration frequency increases, and the dynamic internal friction angle at $f = 3$ Hz is about 7%~12% higher than that at $f = 1$ Hz. Under isotropic consolidation conditions, when the cyclic load is applied and the failure cycles are same, the smaller the vibration frequency, the longer the cycle lasts, and the longer the relative movement of the soil particles and the surrounding free water, resulting in a decrease in the friction of the particles, so that the dynamic internal friction angle of the saturated sand is lower. Under the same failure cycles, the higher the vibration frequency, the shorter the cycle lasts, and the shorter the relative movement of the soil particles and the surrounding free water, resulting in an increase in the friction of the particles, so that the dynamic internal friction angle of the saturated sand is higher. In addition, under the same failure cycles, the higher vibration frequency causes particle breaking, which increases the dynamic internal friction angle of the saturated sand.

In the seismic stability analysis, the static strength parameters c and φ of the soil are often used as inputs, or they are multiplied by a coefficient to replace the dynamic strength parameters c_d and φ_d for seismic stability calculation, but the dynamic strength parameters c_d and φ_d of the soil can actually change with the amplitude, frequency, and failure cycles of the seismic load. Therefore, studying the amplitude, frequency, and duration of seismic load is of great significance to the dynamic strength parameters of sand.

4. Conclusion

The dynamic strength characteristics of saturated sand in the Wenchuan area were studied through the dynamic triaxial

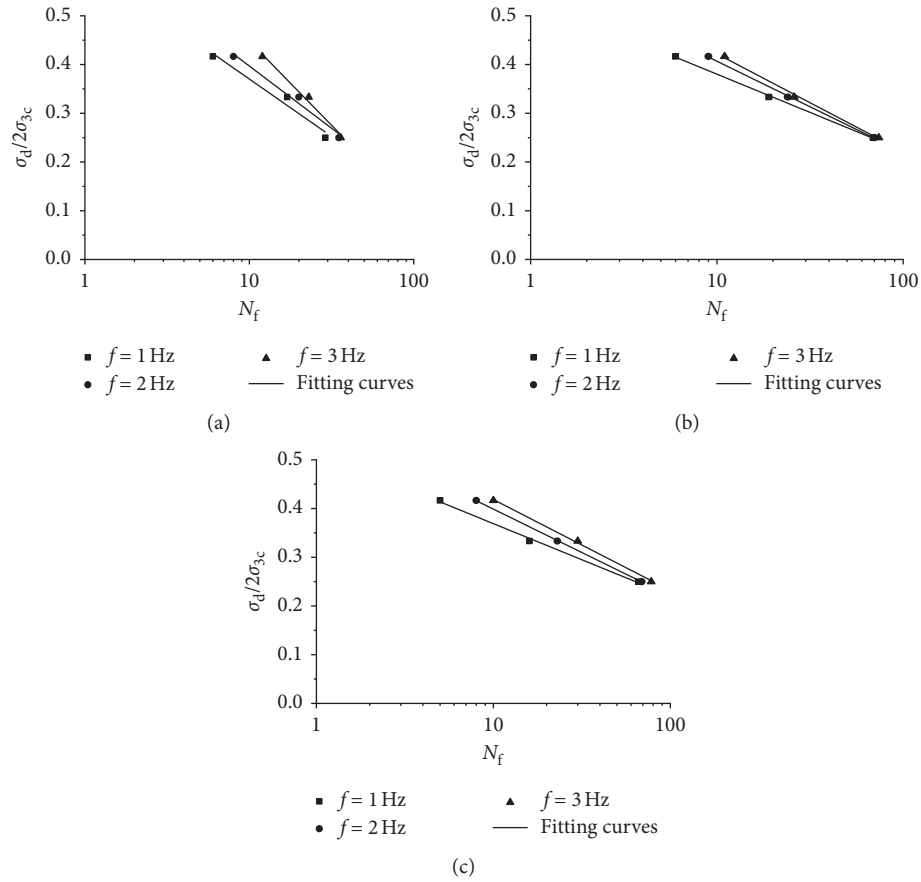

Figure 7: Relationship curves between cyclic stress ratio and failure cycles at different frequencies: (a) $\sigma_{3c} = 50$ kPa; (b) $\sigma_{3c} = 100$ kPa; (c) $\sigma_{3c} = 150$ kPa.

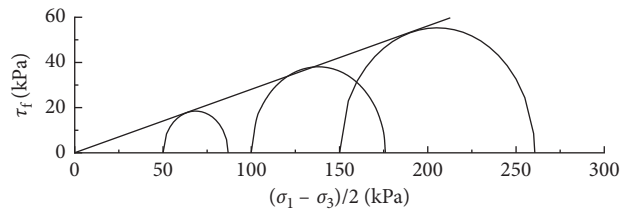

Figure 8: Mohr's circle and strength envelope.

Table 4: Dynamic strength indexes of saturated sand under different cycles.

Frequency (Hz)	1		2		3	
Cycles	φ_d (°)	c (kPa)	φ_d (°)	c (kPa)	φ_d (°)	c (kPa)
10	15.61	0	17.06	1.40	17.26	0.8
20	14.62	2.12	15.97	0	16.30	0
30	14.03	1.80	14.88	1	15.03	0.6

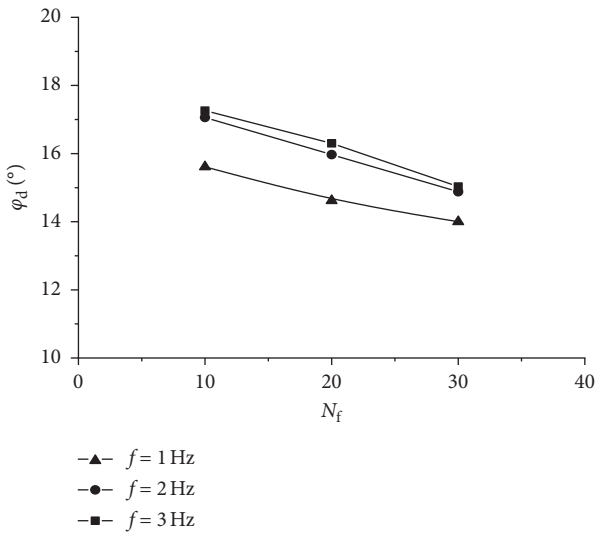

Figure 9: Relationship curves between dynamic internal friction angle and failure cycles at different frequencies.

test system. The influence of initial shear stress, cyclic stress ratio, and vibration frequency on the dynamic strength characteristics of sand was discussed. The results are as follows:

(1) The dynamic strength of saturated sand increases with the increase of confining pressure. Under the same confining pressure and vibration frequency, the dynamic strength of sand increases with the increase of consolidation ratio; when the consolidation ratio exceeds a certain value, the dynamic strength of sand increases slowly instead of increasing indefinitely with the increase of the consolidation ratio.

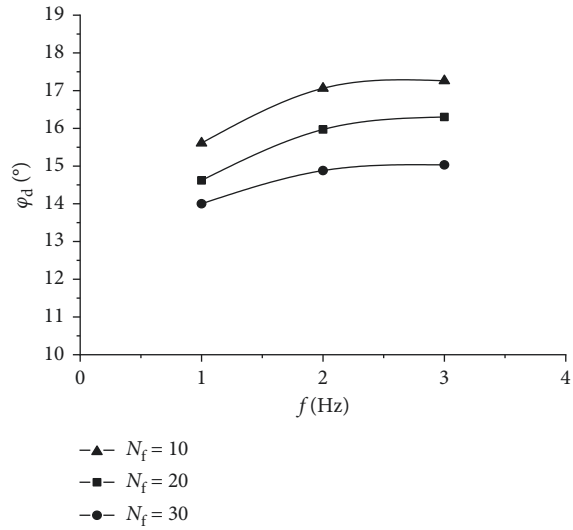

Figure 10: Relationship curves between dynamic internal friction angle and vibration frequency under different cycles.

(2) When the failure cycles is constant, the larger the vibration frequency, the greater the dynamic strength of saturated sand; at the same cyclic stress ratio, the higher the vibration frequency, the greater the cycles required to achieve the failure; and the influence of the vibration frequency on failure cycles is gradually reduced with the decrease of the cyclic stress ratio.

(3) When the vibration frequency is constant, the dynamic internal friction angle first increases and then decreases with the increase of the consolidation ratio; the dynamic internal friction angle under different initial shear stresses differs by a maximum of about 12%.

(4) When the vibration frequency is constant, the dynamic internal friction angle decreases as the cycles increases. When the failure cycle is constant, as the vibration frequency increases, the dynamic internal friction angle of the sand increases. The dynamic internal friction angle at different frequencies differs by a maximum of about 7%.

Data Availability

The data used to support the findings of this study are included within the article.

Conflicts of Interest

The authors declare that there are no conflicts of interest regarding the publication of this paper.

Acknowledgments

The authors are grateful for the financial support from the National Natural Science Foundation of China (no. 51709145) and the Scientific Research Foundation of Nanjing Institute of Technology (YKJ201727).

References

[1] A. B. Fourie and L. Tshabalala, "Initiation of static liquefaction and the role of K0 consolidation," *Canadian Geotechnical Journal*, vol. 42, no. 3, pp. 892–906, 2005.

[2] A. Lashkari, A. Karimi, K. Fakharian, and F. Kaviani-Hamedani, "Prediction of undrained behavior of isotropically and anisotropically consolidated Firoozkuh sand: instability and flow liquefaction," *International Journal of Geomechanics*, vol. 17, no. 10, article 04017083, 2017.

[3] D. Wijewickreme and Y. P. Vaid, "Experimental observations on the response of loose sand under simultaneous increase in stress ratio and rotation of principal stresses," *Canadian Geotechnical Journal*, vol. 45, no. 5, pp. 597–610, 2008.

[4] Y. Yilmaz and M. Mollamahmutoglu, "Characterization of liquefaction susceptibility of sands by means of extreme void ratios and/or void ratio range," *Journal of Geotechnical and Geoenvironmental Engineering*, vol. 135, no. 12, pp. 1986–1990, 2009.

[5] T. Wichtmann and T. Triantafyllidis, "Influence of the grain-size distribution curve of quartz sand on the small strain shear modulus gmax," *Journal of Geotechnical and Geoenvironmental Engineering*, vol. 135, no. 10, pp. 1404–1418, 2009.

[6] D. Porcina, G. Garidi, and V. N. Ghionna, "Undrained monotonic and cyclic simple shear behavior of carbonate sand," *Geotechnique*, vol. 58, no. 8, pp. 635–644, 2008.

[7] G. Suazo, A. Fourie, and J. Doherty, "Effects of confining stress, density and initial static shear stress on the cyclic shear response of fine-grained unclassified tailings," *Geotechnique*, vol. 66, no. 5, pp. 1–12, 2016.

[8] Z. X. Yang and K. Pan, "Flow deformation and cyclic resistance of saturated loose sand considering initial static shear effect," *Soil Dynamics and Earthquake Engineering*, vol. 92, pp. 68–78, 2017.

[9] H. B. Seed and K. L. Lee, "Liquefaction of saturated sands during cyclic loading," *Journal of the Soil Mechanics and Foundations Division*, vol. 92, no. 6, pp. 105–134, 1966.

[10] J. Yang and H. Y. Sze, "Cyclic behaviour and resistance of saturated sand under non-symmetrical loading conditions," *Géotechnique*, vol. 61, no. 1, pp. 59–73, 2011.

[11] V. N. Georgiannou and M. Konstadinou, "Effects of density on cyclic behaviour of anisotropically consolidated Ottawa sand under undrained torsional loading," *Géotechnique*, vol. 64, no. 4, pp. 287–302, 2014.

[12] M. Y. Ma, "Effects of initial consolidation stress on dynamic strength of sands," in *Proceedings of the Geotechnical Buildings and Seismic Behavior of Foundation*, Xi-an, China, September 1986.

[13] K. Pan and Z. X. Yang, "Effects of initial static shear on cyclic resistance and pore pressure generation of saturated sand," *Acta Geotechnica*, vol. 13, no. 2, pp. 473–487, 2018.

[14] R. H. Wang, B. Jia, and A. F. Deng, "Dynamic triaxial testing study on dynamic characteristic of sandy pebble soil," *Chinese Journal of Rock Mechanics and Engineering*, vol. 25, no. 2, pp. 4059–4064, 2006.

[15] Y. F. Gao, J. Zhang, and Y. Shen, "Characteristics of pore water pressure of saturated silt under wave loading," *China Ocean Engineering*, vol. 24, no. 1, pp. 161–172, 2010.

[16] J. T. Cao, Y. G. Sun, and S. J. Huang, "Study of impact of initial void ratio on dynamic behavior of saturated sands," *Journal of China Three Gorges University(Natural Sciences)*, vol. 36, no. 2, pp. 68–71, 2014.

[17] S. J. Huang and J. T. Cao, "Experimental study on effects of initial shear stress on dynamic characteristics of saturated sand of Wenchuan earthquake area," *Journal of Waterway and Harbor*, vol. 38, no. 3, pp. 299–303, 2017.

[18] J. Zhang, J. T. Cao, and S. J. Huang, "Effects of initial shear stress and vibration frequency on the dynamic pore-water pressure of saturated sands," *Advances in Civil Engineering*, vol. 2018, Article ID 6124809, 13 pages, 2018.

[19] Y. P. Vaid, J. D. Stedman, and S. Sivathayalan, "Confining stress and static shear effects in cyclic liquefaction," *Canadian Geotechnical Journal*, vol. 38, no. 3, pp. 580–591, 2001.

[20] X. Z. Yang, X. H. Wang, and J. S. Lei, "Study on dynamic characteristic of saturated sand of XiangJiang river under condition of isotropic consolidation," *Journal of Vibration and Shock*, vol. 26, no. 9, pp. 146–148, 2007.

[21] K. Ishihara, H. Tsuchiya, Y. Huang, and K. Kamada, "Recent studies on liquefaction resistance of sand," in *Proceedings of the 4th International Conference on Recent Advances in Geotechnical Earthquake Engineering and Soil Dynamics*, San Diego, CA, USA, March 2001.

[22] G.-C. Cho, J. Dodds, and J. C. Santamarina, "Particle shape effects on packing density, stiffness, and strength: natural and crushed sands," *Journal of Geotechnical and Geoenvironmental Engineering*, vol. 132, no. 5, pp. 591–602, 2006.

[23] S. Sivathayalan and D. Ha, "Effect of static shear stress on the cyclic resistance of sands in simple shear loading," *Canadian Geotechnical Journal*, vol. 48, no. 48, pp. 1471–1484, 2011.